Research Square

Preprints are preliminary reports that have not undergone peer review.
They should not be considered conclusive, used to inform clinical practice,
or referenced by the media as validated information.

A hybrid electrostatic–plasma filter for energy-efficient air purification and disinfection

Wonho Choe

wchoe@kaist.ac.kr

Korea Advanced Institute of Science and Technology https://orcid.org/0000-0002-8952-8252

Seong-Cheol Huh

Korea Advanced Institute of Science & Technology (KAIST) https://orcid.org/0000-0002-6812-8065

Ki Ho Baek

Korea Institute of Materials Science (KIMS)

Taemin Kang

Korea Institute of Materials Science (KIMS)

Juyeon Choi

Korea Institute of Materials Science (KIMS)

Joo Young Park

Korea Institute of Materials Science (KIMS)

Article

Keywords:

Posted Date: June 23rd, 2026

DOI: https://doi.org/10.21203/rs.3.rs-9941687/v1

License: This work is licensed under a Creative Commons Attribution 4.0 International License.
Read Full License

Additional Declarations: Yes there is potential Competing Interest. Seong-Cheol Huh and Wonho Choe have filed a patent application (10-2025-0004530) for the ESP–SDBD filter concept and are pursuing patent registration.

A hybrid electrostatic–plasma filter for energy-efficient air purification and disinfection

Seong-Cheol Huh[1,§], Ki Ho Baek[2,§], Taemin Kang[2,3], Juyeon Choi[2], Joo Young Park[2], Wonho Choe[1,*]

[1] Department of Nuclear and Quantum Engineering, Korea Advanced Institute of Science and Technology, Daejeon 34141, Republic of Korea

[2] Advanced Bio and Healthcare Materials Research Division, Korea Institute of Materials Science, Changwon 51508, Republic of Korea

[3] Department of Agricultural Biotechnology, Seoul National University, Seoul 08826, Republic of Korea

* Corresponding author: wchoe@kaist.ac.kr

§ These authors contributed equally

Abstract

Energy-efficient and low-waste air disinfection is essential for protecting public health and promoting sustainable development. Here, we present an electrostatic precipitator–surface dielectric barrier discharge (ESP–SDBD) filter that integrates low-power electrostatic collection with plasma-assisted pathogen inactivation. The filter exhibited a 0.1 Pa pressure drop at 600 L/min, continuously captured > 99.994% of airborne *Escherichia coli* and *Micrococcus luteus*, and inactivated > 99.98% of collected bacteria within 1 h. Operational analysis indicates that the ESP–SDBD filter can reduce energy consumption by 30% relative to HEPA filtration. *In situ* reactive species measurements with electrohydrodynamic simulations revealed a synergistic mechanism enhancing inactivation efficacy and energy efficiency by factors of 17.3 and 12.4, respectively, compared with SDBD-only ozonation. These findings highlight the importance of reactive-species utilization, in addition to reactive-species generation, in plasma-assisted disinfection and demonstrate the potential of ESP–SDBD filtration as an energy-efficient and sustainable approach to air purification.

Introduction

Airborne pathogens, including bacteria, viruses, and fungi, transmit infectious diseases such as influenza, measles, and tuberculosis via respiratory aerosols[1]. Such pathogens can remain viable in the air for hours and travel tens of meters being carried by aerosols with diameters of 5–10 μm or smaller, substantially expanding the zone of exposure[2]. The catastrophic public health and macroeconomic impacts of such diseases were underscored by the COVID-19 pandemic, which caused over 7 million documented fatalities and severe global economic contraction[3,4]. Recurrent epidemics of airborne strains such as H1N1 influenza generate cumulative macroeconomic damages estimated at hundreds of billions of USD through healthcare costs and lost productivity[5]. Beyond human health, airborne diseases threaten food security as well, exemplified by foot-and-mouth disease being responsible for global livestock losses estimated between 6.5 and 21 billion USD annually[6]. These examples underscore the importance of preventing airborne pathogen transmission to protect public health and promote sustainable development.

Air disinfection technologies are critical for preventing the transmission of airborne pathogens in indoor environments. Conventional technologies for air purification include high-efficiency particulate air (HEPA) filters, ultraviolet lamps, activated carbon filters, and electrostatic precipitators (ESPs), among which HEPA filtration is the most widely used[7]. HEPA filters remove particulate matter with diameters of 0.3 μm or larger at an efficiency of 99.97% by mechanically capturing pollutants through collisions with a dense network of polypropylene or fiberglass fibres[8]. HEPA filters are effective in mitigating allergens and pathogens and have been shown to reduce respiratory symptoms in sensitive populations[9,10]. However, HEPA filters have significant disadvantages, including high energy consumption, waste generation from single-use disposable filters, and potential risks of recontamination. High energy consumption results from pressure losses that increase from ≥ 250 Pa initially to 500–1000 Pa as particulate matter accumulates on the filter, at which point replacement is required, producing non-reusable and largely non-recyclable waste[8,11]. Because HEPA filters do not possess inherent inactivation mechanisms, microorganisms captured on the filters can survive for extended periods: *Bacillus atrophaeus* spores have survived for up to 210 days, *Aspergillus brasiliensis* and MS-2 bacteriophage have survived for 6–7 days, and *Staphylococcus epidermidis* has remained viable for up to 6 days[12]. This survival poses serious risks of pathogen re-aerosolisation during HEPA filter replacement[13]. With the global HEPA filter market valued at approximately 0.4 billion USD and

compounding at 7% annually[14], the associated energy consumption and generation of biohazardous, non-recyclable waste are expected to increase substantially. Consequently, there is a growing need for alternative self-disinfecting air filtration technologies with lower energy consumption and waste generation.

In recent years, numerous non-thermal plasma-based filtration technologies have been proposed for self-disinfecting air purification systems[15]. These plasma filters can be broadly categorised into two groups according to their approach to airborne pathogen inactivation: instantaneous inactivation within the airflow by direct plasma exposure[16–18], or plasma-based inactivation of pathogens captured on solid media[19–22]. In the former approach, plasma fills the entire cross-section of a duct section, directly exposing the airflow and inactivating pathogens on a millisecond timescale as the air passes through the plasma. In the latter approach, a plasma device inactivates pathogens captured on solid media within or downstream of the device, commonly on dielectric beads filling the device or on a HEPA filter installed downstream. The agents responsible for pathogen inactivation in these devices include reactive oxygen species (O_3, H_2O_2, •OH, $^1O_2$), reactive nitrogen species (NO, NO_2, NO_3^-, N_2O_5), charged particle bombardment, and strong local electric fields, which inactivate pathogens through mechanisms such as lipid peroxidation, protein modification, electrostatic disruption, or electroporation[23–25].

Although plasma filter technologies can substantially reduce waste generation and recontamination risks compared with HEPA filters, their real-world application has been limited, in part, by the requirement for increased energy input. In plasma filters employing direct plasma exposure, considerable power is required to sustain a discharge large enough to encompass the entire duct cross-section and sufficiently intense to inactivate airborne pathogens instantaneously as they pass through the plasma. When combined with the requirement for continuous plasma discharge during airflow, lowering the total energy consumption relative to HEPA filtration through this approach is challenging. Alternatively, plasma filters operating in conjunction with solid media can mitigate plasma power requirements by extending the treatment time for captured pathogens, thereby reducing the required plasma volume and intensity. However, reliance on mechanical capture by solid media introduces pressure losses that, when combined with plasma energy consumption, result in total energy demands comparable to those of HEPA filtration. Consequently, achieving lower total energy consumption than HEPA filtration remains a critical objective in the development of practical plasma filter technologies.

ESPs are another class of air purification technology that has been widely investigated for airborne pathogen reduction because they can achieve high particle collection efficiency with low pressure drop and energy consumption[26–28]. In a typical ESP, airborne particulate matter is electrically charged in a corona discharge and then directed onto collecting plates by electrostatic forces[29]. ESPs are capable of efficiently capturing airborne particles, with filtration efficiencies exceeding 95–99.9% for submicron particles and pressure drops of a few to a few tens of Pa[30,31]. However, the intrinsic inactivation capability of conventional ESPs is limited: survival rates of collected *Staphylococcus aureus* were reported to exceed 60% in the downstream section of a two-stage ESP, owing to low reactive species concentrations at locations distant from the corona discharge[28]. It has been shown that ESP inactivation performance can be enhanced by using antiviral copper collecting plates, achieving up to 99.9% inactivation of bacteriophage Φ6 after 2 hours of contact[32]; however, the effectiveness of such passive inactivation against more resistant pathogens, including bacteria and fungi, remains uncertain[33]. Therefore, alternative strategies are required to improve the performance of ESP devices.

While reactive oxygen and nitrogen species generated by non-thermal plasmas are widely recognized as the primary agents responsible for pathogen inactivation[23–25], disinfection performance is often assessed primarily through plasma power or reactive-species concentration. However, the transport of reactive species from the plasma generation region to contaminated surfaces may also play a critical role in determining overall efficacy. Previous studies have shown that electric wind can enhance antimicrobial performance in plasma-based air treatment systems[34,35]. However, these studies primarily focused on airborne microorganisms treated directly in the airflow. The role of electrohydrodynamic transport in hybrid collection–disinfection systems, where pathogens are first captured on surfaces and subsequently inactivated, remains poorly understood.

In this work, we introduce an electrostatic precipitator–surface dielectric barrier discharge (ESP–SDBD) plasma filter and evaluate its air disinfection performance. The ESP–SDBD filter has a simple structure that directly embeds plasma sources within an ESP, resulting in a minimal pressure drop of 0.1 Pa at a volumetric flow rate of 600 L/min. The proposed filter captures airborne pathogens using 30% less energy than HEPA filters and inactivates collected pathogens with less than half the energy stored in a typical smartphone battery, thereby overcoming the high energy demands of both HEPA filters and alternative plasma-based

approaches. All components of the ESP–SDBD filter are reusable, eliminating disposable waste generation. The collection and inactivation performance were assessed at an airflow rate of 600 L/min using aerosolised *Escherichia coli* (*E. coli*) and *Micrococcus luteus* (*M. luteus*). Pathogen removal from the airstream and inactivation on internal filter surfaces were quantified through outflow air sampling and surface sampling, respectively. Analysis of measured *in situ* reactive species concentrations, combined with simulations of convective gas flow induced by electric wind, reveals a synergistic mechanism that increases inactivation efficacy by more than 17-fold and energy efficiency by more than 12-fold compared with SDBD-only ozonation treatment. The ESP–SDBD filter achieved more than 99.994% continuous removal of bacterial aerosols from the airstream and more than 99.98% inactivation of collected bacteria within one hour, demonstrating its potential as an energy-efficient and scalable approach to advanced air purification.

Results

ESP–SDBD plasma filter

The concept and structure of the ESP–SDBD filter are illustrated in Fig. 1a. The ESP–SDBD filter is based on a two-stage ESP, segmented into a charging section at the front and a collecting section at the rear. In the charging section, corona discharges form between the grounded charging wires and the metal charging plates when a high DC voltage is applied to the plates. These corona discharges electrically charge pathogens in the inflowing airstream. The collecting section integrates surface dielectric barrier discharge (SDBD) units between the metal collecting plates. The grid electrodes on both sides of each SDBD unit are grounded, whereas the metal collecting plates are charged with a high DC voltage of the same polarity as the charging plates. This arrangement creates a static electric field in the collecting section that guides the charged pathogens onto the collecting plates, thereby removing them from the airstream while allowing the SDBD units to generate SDBD plasma independently of the pathogen collection process. The SDBD units are powered by high AC voltage applied to the sheet electrodes in the centre of the SDBD units.

The SDBD units generate plasma and directly supply ozone (O_3) within the ESP–SDBD filter to inactivate the collected pathogens. Each SDBD unit consists of two SDBD sources assembled together. Each SDBD source comprises a thin dielectric film with a rectangular grid electrode on one side and a rectangular sheet

electrode on the other side (Fig. 1b). The electrodes are fabricated by screen printing and sintering silver paste ink onto the dielectric films. Each SDBD unit is assembled by placing two SDBD sources together with the sheet electrodes facing each other, such that the grid electrodes face outwards.

The ESP–SDBD plasma filter used in this study is compatible with square ducts having an internal cross-section of 100 × 100 mm^2. The interior is segmented into five identical channels, with the charging and collecting plates forming the boundaries of each channel (Fig. 1c). One charging wire and one SDBD unit are positioned in each channel at equal distances from the charging plates and collecting plates, respectively.

Airborne bacteria collection

The results of the airborne bacteria collection experiments are presented in Fig. 2a–c. The aerosol size distributions of *E. coli* and *M. luteus* are shown in Fig. 2a. Although the aerosol number density of *E. coli* was higher than that of *M. luteus*, the size distributions were similar between the two species, with most aerosols distributed between 0.65 and 2.1 μm. Specifically, 33% and 61% of *E. coli* aerosols were within the 0.65–1.1 μm and 1.1–2.1 μm ranges, respectively, whereas the corresponding values for *M. luteus* were 38% and 57%.

The results of the airborne *E. coli* and *M. luteus* collection experiments are presented in Fig. 2b and Fig. 2c, respectively. In both experiments, no viable bacteria were detected downstream of the ESP–SDBD filter during ESP or ESP + SDBD operation, whereas SDBD-only operation did not improve aerosol removal relative to the control. The SDBD and ESP + SDBD conditions were tested to evaluate whether convective airflow induced by electric wind, blowing perpendicularly from the surface of the SDBD units[36], might either enhance or hinder the collection of airborne bacteria. During preliminary testing conducted prior to assembling the SDBD units, no electric wind was detected near the SDBD source surfaces using a handheld anemometer, indicating that any electric wind generated solely by the SDBD sources was weak, with a velocity of less than 1 m/s. Nevertheless, airborne *E. coli* and *M. luteus* exhibited a slight increase in downstream viable bacterial concentration during SDBD operation relative to the control group (Supplementary Table 1).

These observations suggest that weak SDBD-induced airflow may have altered the local flow conditions within the collecting section; however, the present data do not directly distinguish between reduced

deposition within the device and reduced net removal from the airstream. By contrast, ESP operation was effective in bacterial aerosol collection. Taking the common limit of detection (LOD; 1.25 log CFU/m^3) into account, the reduction in downstream viable bacterial concentration exceeded 4.61 log CFU/m^3 for *E. coli* and 4.25 log CFU/m^3 for *M. luteus* relative to the control. These values correspond to collection efficiencies exceeding 99.998% and 99.994%, respectively. Because both ESP and ESP + SDBD yielded non-detectable downstream counts, whereas ESP alone required lower power input, ESP operation was considered the most energy-efficient mode for bacterial aerosol collection in the present system.

Collected bacteria inactivation

The results of the collected bacteria inactivation experiments are presented in Fig. 2d. Only results for *M. luteus* are shown because *E. coli* remained below the detection limit under all experimental conditions, including the control group. In a follow-up experiment, *E. coli* also remained undetectable when the ESP–SDBD metal plates were removed and surface-sampled immediately after 30 min of aerosol spraying and ESP collection, suggesting rapid inactivation of collected *E. coli* during the collection step. By contrast, *M. luteus* remained recoverable in the control group, with mean surface densities of 3,443 CFU/cm^2 and 369 CFU/cm^2 on the charging and collecting plates, respectively. The average inactivation efficacy, in increasing order, was ESP < SDBD < ESP + SDBD in the charging section, whereas it was ESP ≈ SDBD < ESP + SDBD in the collecting section (Supplementary Table 2).

The observed 1.57 and 2.33 log reductions achieved by ESP operation indicate that corona discharge alone provided a measurable degree of inactivation but was insufficient for satisfactory disinfection of the ESP–SDBD filter. Notably, the reduction of *M. luteus* was greater in the collecting section than in the charging section during ESP operation, contrary to expectations, as the corona discharge responsible for bacterial inactivation was primarily confined to the charging section. One plausible explanation is a shielding effect, whereby extensive deposition of bacteria and residual salt in the charging section formed multilayer deposits that partially protected underlying cells from corona-induced inactivation[37].

SDBD operation achieved a markedly higher 3.20 log reduction in the charging section compared with ESP operation but did not outperform ESP operation in the collecting section, yielding a 2.38 log reduction of collected *M. luteus*. As shown in Fig. 2d, the level of remaining *M. luteus* under SDBD operating

conditions was not lower in the collecting section than in the charging section, despite the control results being an order of magnitude lower in the collecting section than in the charging section. These findings suggest the presence of a lower inactivation limit for SDBD operation, beyond which further pathogen inactivation is difficult to achieve by SDBD alone. This limitation may arise from the chemical nature of the SDBD inactivation mechanism, which relies on long-lived reactive species such as O_3 or dinitrogen pentoxide (N_2O_5) generated by the SDBD to inactivate pathogens through oxidation[38,39]. Although effective to a certain extent, oxidation alone may be insufficient to achieve complete inactivation.

ESP + SDBD operation achieved the highest level of inactivation, reducing collected *M. luteus* by 3.88 log and 3.61 log on the charging and collecting plates, respectively. This corresponds to inactivation rates of 99.99% and 99.98% on the charging and collecting plates, respectively. Notably, *M. luteus* was not detectable on the upper surface of the bottom charging plate or on the lower surface of the top collecting plate. In particular, for the collecting plates, the 3.61 log reduction achieved by ESP + SDBD operation represented a 17.3-fold increase in inactivation efficacy compared with the 2.38 log reduction achieved by simple ozonation during SDBD operation. These results indicate that the combined operation of the ESP and SDBD components overcomes their individual limitations, resulting in enhanced disinfection. We conclude that ESP + SDBD operation is the most effective operating mode for collected bacteria inactivation in the ESP–SDBD filter.

Power consumption and energy efficiency

The power consumption of the ESP–SDBD filter is presented in Fig. 3a. The power consumption of the ESP component remained constant at 2.66 ± 0.01 W during 30 minutes of 1 m/s duct airflow, whereas it gradually decreased from 2.69 to 1.82 W during a 1-hour discharge under zero duct airflow. Meanwhile, the power consumption of the SDBD component gradually decreased from 5.6 to 4.5 W during a 1-hour discharge under zero duct airflow. This gradual decrease in the power consumption of the ESP and SDBD components during the 1-hour discharge in still air appears to be attributable to an increase in air temperature during sustained discharge[40,41]. The energy consumption during the 1-hour bacterial inactivation period was 1.99, 4.8, and 6.8 Wh for the ESP, SDBD, and ESP + SDBD operating modes, respectively (Fig. 3b). For context, this value is less than half the energy stored in a Samsung Galaxy S25 FE smartphone battery (4755 mAh)

with a nominal voltage of 3.88 V, corresponding to an energy capacity of 18.45 Wh. These results highlight the low energy consumption of the ESP–SDBD filter.

The inactivation energy efficiency of collected *M. luteus* under the various operating modes of the ESP–SDBD filter is presented in Fig. 3b and Table 1. A comparison of the inactivation efficiencies of ESP and SDBD operation revealed mixed results, with SDBD operation providing higher efficiency in the charging section, whereas ESP operation provided higher efficiency in the collecting section. These differences can be attributed to the limitations of each method discussed in the previous section, as well as to the 2.4-fold higher energy consumption of the SDBD component compared with the ESP component during the 1-hour bacterial inactivation period. By contrast, combined ESP + SDBD operation achieved substantially higher inactivation efficiencies than either method alone, exceeding SDBD operation threefold in the charging section and exceeding ESP operation fivefold in the collecting section. Notably, the inactivation efficiency of ESP + SDBD operation in the collecting section was 12.4-fold higher than that achieved by SDBD operation representing simple ozonation. The higher level and efficiency of inactivation achieved by ESP + SDBD operation compared with ESP or SDBD operation alone indicate a synergistic effect between the ESP and SDBD components in bacterial inactivation. We conclude that ESP + SDBD operation is the most efficient operating mode for collected bacteria inactivation in the ESP–SDBD filter.

Reactive species concentration measurements

Under 1 m/s duct airflow conditions used in the collection experiments, the steady-state O_3 concentration downstream of the ESP–SDBD filter outlet was 0.88 ppmv (Supplementary Fig. 1). Under zero duct airflow conditions used in the inactivation experiments, the O_3 concentration within the ESP–SDBD filter was measured *in situ* to elucidate the mechanism of inactivation and to explain the synergistic effect between the ESP and SDBD components in the inactivation of collected bacteria. The results of the *in situ* reactive species measurements obtained by broadband UV–visible absorption spectroscopy under zero duct airflow conditions are presented in Fig. 4a–c. For the SDBD and ESP + SDBD operating modes, N_2O_5 was also detected and plotted alongside O_3. As expected, ESP operation yielded the lowest O_3 concentration, with a steady-state value (20–60 min average) of 20.8 ppmv, whereas SDBD operation produced a substantially higher O_3 concentration, with a steady-state value of 686 ppmv. This higher O_3 concentration explains the

overall enhancement of *M. luteus* inactivation during SDBD operation compared with ESP operation. However, contrary to expectations, the O_3 concentration during ESP + SDBD operation was more than 80% lower than that during SDBD operation, with a steady-state value of only 126.7 ppmv, despite ESP + SDBD operation exhibiting the highest inactivation efficacy and efficiency among all operating modes. These findings indicate that O_3 concentration alone cannot account for the synergistic effect between the ESP and SDBD components in the inactivation of collected bacteria.

To verify that the reduced O_3 concentration observed during ESP + SDBD operation under zero duct airflow was a genuine effect rather than a measurement artefact, an "ESP switching" experiment was conducted. In this experiment, the SDBD was continuously discharged for 1 hour under zero duct airflow, while the ESP component was periodically activated for 30 s every 5 min and then deactivated. The results of the ESP switching experiment are presented in Fig. 4d. During periods when the ESP component was switched off, the concentrations of O_3 and N_2O_5 approached the levels observed during SDBD operation (Fig. 4b). However, when the ESP component was switched on, the O_3 and N_2O_5 concentrations rapidly decreased to levels comparable to those measured during the ESP + SDBD operation experiments (Fig. 4c). Because ESP operation itself produced O_3 (Fig. 4a), it was unlikely that activation of the ESP component during SDBD operation destroyed O_3 within the ESP–SDBD filter. After excluding alternative explanations, the most plausible interpretation was that electric wind generated during ESP + SDBD operation reduced the O_3 and N_2O_5 concentrations by transporting these reactive species. However, this experiment alone could not determine the origin or direction of the electric wind, thereby motivating a numerical simulation study.

Simulation and mechanism of inactivation enhancement

The simulation results of the electric wind during ESP + SDBD operation under zero duct airflow are presented in Fig. 5. We initially hypothesised that the electric wind generated by the corona discharge of the ESP component[42] reduced O_3 concentrations by transporting O_3 out of the ESP–SDBD filter. However, preliminary simulation results modelling only the corona discharge indicated that the electric wind induced by the corona discharge was confined to the charging section. This finding prompted consideration of an alternative source of electric wind present only during ESP + SDBD operation. According to Equation (9) in the Methods section, electric wind arises in regions where space charges experience drift under an electric

field, thereby transferring momentum to neutral species. In our experimental setup, activation of the ESP component established an electric field between the SDBD units and the collecting plates because the ESP power module was connected to both electrodes (Fig. 5a). If the SDBD units supplied ions as space charges within the collecting section (Fig. 5b), this electric field would drive an electric wind from the SDBD units towards the collecting plates, thereby transporting O_3 and N_2O_5 onto the plates. As shown in Fig. 5c, an electric wind simulation model comprising both the corona discharge in the charging section and the SDBD in the collecting section confirmed the existence of electric wind directed from the plasma towards the metal plates in both sections. This mechanism, further illustrated in Fig. 6, consistently explains both the reduced concentrations of these reactive species and the higher inactivation efficacy and efficiency of collected *M. luteus* during ESP + SDBD operation.

Along with the results of the electric wind simulation, prior experimental studies reported in the literature provide further supporting evidence. Electric wind flowing from an SDBD source towards a parallel DC-biased metal plate has been visualised by injecting sulfuric acid aerosols into an airflow between the SDBD source and the metal plate, and ion injection from the SDBD into the gap has been quantified by measuring the ion current collected at the metal plate[43,44]. The positive and negative ion densities in the airstream flowing out from between an SDBD source and a parallel DC-biased metal plate have been measured, leading to the conclusion that applying a DC bias to the metal plate attracts ions of opposite polarity towards the metal plate and creates electric wind[34]. Prior research shows that SDBDs are bipolar ion sources of water cluster ions $M \cdot (H_2O)_n$, where M can represent positive ions such as H_3O^+, NO^+, or NO_2^+, or negative ions such as O_3^-, OH^-, CO^-, O_2^-, CO_3^-, NO_2^-, NO_3^-, or HCO_3^-[45–48]. We therefore conclude that the enhanced inactivation efficacy and efficiency observed for ESP + SDBD operation, relative to ESP or SDBD operation alone, result from synergy between increased reactive species production by the SDBD and enhanced transport of these species to the charging and collecting plates by corona-discharge-induced and SDBD–plate-induced electric wind, respectively.

Discussion

A notable outcome of this study is that the ESP + SDBD operating mode exhibiting the highest bacterial inactivation efficacy and energy efficiency produced lower ozone concentrations than simple ozonation. This

observation indicates that reactive-species concentration alone is insufficient to explain disinfection performance in the ESP–SDBD filter. Instead, the combined experimental and computational results suggest that reactive-species transport plays a critical role. While simple ozonation relies primarily on diffusion to deliver reactive species to contaminated surfaces, combined ESP + SDBD operation generates electrohydrodynamic flow that actively transports plasma-generated reactive species toward the charging and collecting plates. Consequently, a larger fraction of the generated reactive species can participate in pathogen inactivation rather than being lost through dilution or decomposition. These findings suggest that improving reactive-species utilization may be as important as increasing reactive-species production when designing energy-efficient plasma disinfection systems.

Compared with HEPA filtration, ESP–SDBD filtration reduces energy consumption, adds pathogen inactivation capability, and decreases waste from consumables. Typical HEPA filters have pressure drops of approximately 250 Pa, airflow velocities of approximately 1 m/s, and dimensions on the order of tens of centimetres[8,49]. The pressure drop across HEPA filters increases with use as particulate matter accumulates on the filter, reaching 500–1000 Pa by the end of the service life. A HEPA filter with a 60 × 60 cm^2 cross-section, 1 m/s airflow, and a linearly increasing pressure drop from 250 to 500 Pa during continuous operation for 180 days would consume 583 kWh of energy, not accounting for fan efficiency losses. By comparison, the pressure loss of the ESP–SDBD filter was 0.1 Pa. If the ESP–SDBD filter were scaled to a 60 × 60 cm^2 cross-section, operated continuously in ESP mode at 1 m/s for 180 days, and subsequently subjected to ESP + SDBD operation for 2 hours under still-air conditions for collected pathogen inactivation, the total energy expenditure would be 414 kWh, representing a 30% reduction in energy consumption compared with the equivalent HEPA filter case. By adopting a strategy of selecting the most energy-efficient operating mode for airborne pathogen collection and collected pathogen inactivation, the ESP–SDBD filter can overcome the limitations of existing plasma-based inactivation technologies and achieve lower energy consumption than HEPA filtration.

Nevertheless, there remains considerable scope for improvement of the ESP–SDBD filter. One critical issue that must be addressed before real-world application is the reduction of O_3 concentration during airborne pathogen collection operation. The steady-state O_3 concentration of air downstream of the ESP–SDBD filter in this study, at 1 m/s duct airflow, was 0.88 ppmv (880 ppbv). By comparison, World Health

Organization guidelines require the daily maximum 8-hour average O_3 concentration to be 100 μg /m^3 (approximately 50 ppbv) or lower[50], whereas the National Ambient Air Quality Standards require the O_3 concentration to be 70 ppbv or lower[51]. Therefore, the O_3 concentration produced by the ESP–SDBD filter during airborne pathogen collection operation must be reduced approximately 18-fold before real-world application. This issue could be addressed by replacing the metal wire in the charging section with carbon brushes or other sharp electrodes[52,53], or by adopting optimised conventional ESP designs. For example, a two-stage ESP with a carbon brush ioniser achieved 95% collection efficiency for 0.25–0.35 μm particles at 1 m/s airflow, with O_3 concentrations below 20 ppbv[31]. A two-stage conventional ESP with 0.1 mm diameter tungsten wires attained a collection efficiency exceeding 99.9% for 300 nm particles and exceeding 99.3% for 10–25 nm particles at 1 m/s airflow, with O_3 concentrations of 62 ppbv and a power consumption of 1.75 W[3030]. As demonstrated in these examples, it should be possible to reduce the O_3 concentration of the ESP–SDBD filter during airborne pathogen collection operation to below regulatory limits by adopting advanced ionisation techniques and optimising filter design. Such a reduction in O_3 production by the ESP component would have minimal impact on ESP + SDBD pathogen inactivation operation, as the SDBD is the dominant source of reactive species. This is evidenced by the two orders of magnitude difference in O_3 concentration measured under zero duct airflow conditions during ESP operation (Fig. 4a) and SDBD operation (Fig. 4b).

Another potential issue is the variability of reactive species produced by the SDBDs with humidity. The composition of reactive species generated by dielectric barrier discharges varies with humidity. Specifically, O_3 production is favoured under low-humidity conditions, whereas the production of short-lived OH, H_2O_2, and HO_2 radicals is favoured under high-humidity conditions[54–57]. Although OH, H_2O_2, and HO_2 radicals are highly oxidative and more effective than O_3 in inactivating pathogens, their lifetimes in air are correspondingly short, and they may not reach the metal plate surfaces before dissipating. Therefore, it is difficult to predict in advance whether higher or lower humidity conditions will be beneficial for collected pathogen inactivation. Nevertheless, even if greater power is required for inactivation at certain humidity levels, the overall energy efficiency of the ESP–SDBD filter is unlikely to change substantially, because the inactivation time is negligible compared with the collection time; consequently, the overall energy efficiency converges towards the collection efficiency. Comprehensive testing across a wide range of humidity conditions should be conducted to optimise SDBD operation prior to real-world application of the ESP–

SDBD filter.

In this study, an ESP–SDBD filter integrating SDBD sources into the collecting section of a two-stage ESP was developed for the collection and inactivation of airborne pathogens. The filter is fully reusable through simple washing to remove collected particulate matter from its internal surfaces. At an airflow rate of 600 L/min, the ESP–SDBD filter achieved 99.998% and 99.994% removal of airborne *E. coli* and *M. luteus*, respectively, instantaneously inactivated collected *E. coli* to below the limit of detection, and inactivated collected *M. luteus* by up to 99.99% after 1 h of operation under still-air conditions. Power consumption remained low, at 2.66 W during airborne pathogen collection and an average of 6.8 W during collected pathogen inactivation. Notably, combined ESP + SDBD operation improved bacterial inactivation efficacy and energy efficiency by factors of 17.3 and 12.4, respectively, compared with simple ozonation. Experimental measurements and numerical simulations indicate that this enhancement resulted from a synergistic interaction between reactive-species generation and electrohydrodynamic transport, which increased the delivery of plasma-generated reactive species to contaminated collection surfaces. Operational energy efficiency was further improved by decoupling pathogen collection and inactivation, enabling a 30% reduction in energy consumption relative to HEPA filtration while eliminating disposable filter waste. Beyond demonstrating a practical and scalable air disinfection technology, these findings highlight the importance of reactive-species transport and utilization, in addition to reactive-species generation, in determining the performance of plasma-assisted disinfection systems.

Methods

ESP–SDBD filter characterisation

The ESP–SDBD plasma filter used in this study was compatible with square ducts having an internal cross-section of 100 × 100 mm^2. Tungsten wires with a diameter of 0.1 mm were used as charging wires, while 1 mm-thick stainless steel plates were used as the charging and collecting plates. The exposed areas of the charging and collecting plates were 60 × 100 mm^2 and 100 × 150 mm^2, respectively. Polycarbonate spacers with a length of 10 mm were inserted between the charging and collecting plates to separate the charging and collecting sections. Kapton sheets with a thickness of 125 μm and silver paste ink (InkTec TEC-PA-060)

were used to fabricate SDBD sources with an exposed area of 100 × 150 mm^2. Fused silica windows (1 mm thick) were attached to both sides of the collecting section of the first channel for broadband UV–visible absorption spectroscopy. The casing of the ESP–SDBD filter was made of polycarbonate. The total length of the ESP–SDBD filter was 250 mm, including the external flanges used to install the filter between the ducts.

Experimental setup

The experimental setup used in this study is illustrated in Supplementary Fig. 2. The ESP–SDBD filter was installed in the middle of a 1.5 m-long duct with an internal cross-section of 100 × 100 mm^2 (Supplementary Fig. 2a). Both ends of the duct were fitted with HEPA filters to prevent unintended air contamination. Indoor air was drawn into the duct at a velocity of 1 m/s, corresponding to a volumetric flow rate of 600 L/min, by a centrifugal blower. The aerosol inlet was located 0.50 m upstream of the ESP–SDBD filter inlet, while the aerosol outlet was located 0.15 m downstream of the ESP–SDBD filter outlet. Two pressure ports, positioned 100 mm upstream and downstream of the ESP–SDBD filter inlet and outlet, respectively, were used to measure the pressure drop across the plasma filter using a differential pressure transducer. Air temperature and relative humidity were monitored using a digital thermo-hygrometer.

The ESP charging and collecting functions of the ESP–SDBD filter were powered by an adjustable high-voltage DC supply module (ESDEMC, HVM-A103.13P12M) set to a +6.0 kV DC output. The SDBD units were powered by a custom high-voltage amplifier that transformed a 60 Hz, 220 V_{rms} input into a 60 Hz, 2.340 kV_{pp} sinusoidal voltage. A 1000:1 high-voltage probe was used to measure the voltage applied to the sheet electrodes of the SDBD units, while a 0.1 V/A Rogowski coil was used to measure the current flowing through the SDBD units. A digital oscilloscope and a multimeter were used to monitor the SDBD and ESP component voltage and current data, respectively. The power dissipated by the corona discharge and the SDBD was calculated by multiplying the corresponding voltages and currents. Average power data over 12 discharge periods were recorded for the SDBD, whereas single-measurement power data were recorded for the corona discharge. The voltage and current waveforms of the SDBD units are provided in Supplementary Fig. 3.

Two different setups were used to measure the O_3 concentration within the ESP–SDBD filter. Under 1 m/s

duct airflow conditions used in the collection experiments, an O_3 monitor (2B Technologies, 106-L) with a maximum flow rate of 1.5 L/min was connected to the duct aerosol outlet to measure the O_3 concentration within the filter. Under zero duct airflow conditions used in the inactivation experiments, *in situ* broadband UV–visible absorption spectroscopy was employed to measure O_3 concentrations within the ESP–SDBD filter (Supplementary Fig. 2b). Two collimating lenses (Ocean Optics, 74-UV) were positioned opposite each other across the fused silica windows of the ESP–SDBD filter. One lens was connected to a deuterium–halogen lamp, while the other lens was connected to a UV–visible spectrometer (Ocean Optics, Maya2000 Pro) via optical fibres. The spectrometer recorded 2068 wavelengths ranging from 200.1 to 1100.5 nm, with eight spectra averaged at an integration time of 125 μs, resulting in a time resolution of 1 s. The measured data were exported to a desktop computer, and spectral data at 415 wavelengths from 210.3 to 399.7 nm were used for broadband UV–visible absorption spectral deconvolution[58] to determine the concentrations of O_3 and N_2O_5 at the mid-plane of the ESP–SDBD filter.

Experimental conditions and procedure

All experimental results in this study were obtained in triplicate. Three types of experiments were conducted: airborne bacteria collection, collected bacteria inactivation, and O_3 measurement. For each type of experiment, three operating modes were defined: ESP, SDBD, and ESP + SDBD operation. ESP operation was defined as the application of +6.0 kV DC to the charging and collecting plates, thereby generating a corona discharge in the charging section while the sheet electrodes of the SDBD units were grounded. SDBD operation was defined as the application of a 60 Hz, 2.340 kV_{pp} sinusoidal voltage to the sheet electrodes of the SDBD units, thereby generating SDBD plasma on the surfaces of the units while the charging and collecting plates were grounded. ESP + SDBD operation was defined as the simultaneous application of +6.0 kV DC to the charging and collecting plates and a 60 Hz, 2.340 kV_{pp} sinusoidal voltage to the sheet electrodes of the SDBD units, thereby activating all plasma discharges within the ESP–SDBD filter. During the control experiments for airborne bacteria collection and collected bacteria inactivation, all electrodes within the ESP–SDBD filter were grounded; consequently, no plasma discharge occurred.

The procedures for the airborne bacteria collection and collected bacteria inactivation experiments are summarised in Supplementary Fig. 4. For the airborne bacteria collection experiments, the duct airflow was

set to 1 m/s and the ESP–SDBD filter was operated in the designated mode. The system was allowed to run for 2 minutes to stabilise the airflow and plasma discharge. Subsequently, bacterial aerosol was sprayed into the duct for 20 seconds to achieve stabilisation, and airborne bacteria were sampled using an impactor for a predetermined duration depending on the experimental condition. Afterwards, the impactor and atomiser were switched off, the agar plates within the impactor were removed for incubation, and the system was reset. For the collected bacteria inactivation experiments, the duct airflow was set to 1 m/s and the ESP–SDBD filter was initially operated in ESP mode. The system was allowed to run for 2 minutes to stabilise the airflow and plasma discharge. Bacterial aerosol was then sprayed into the duct for 30 minutes to accumulate sufficient bacteria on the charging and collecting plates of the ESP–SDBD filter. After 30 minutes of collection, the atomiser was switched off, and a 20-second interval was allowed to release residual pressure and aerosols. Following this transition period, the duct airflow was switched off and the ESP–SDBD filter was simultaneously set to the designated operating mode, after which post-collection treatment continued for 1 hour. After post-collection treatment, the ESP–SDBD filter was switched off and removed from the duct. The charging and collecting plates were then removed for surface sampling, and the system was reset. The power consumption and pressure drop of the ESP–SDBD filter were measured during the collected bacteria inactivation experiments.

Because humidity can affect the O_3 production[59] and inactivation performance[60,61] of SDBDs, control of air humidity was necessary to ensure consistent results. During the airborne bacteria collection and collected bacteria inactivation experiments, the indoor air temperature and relative humidity were maintained within the ranges of 21–23 °C and 45–55%, respectively. For the O_3 measurement experiments conducted at 1 m/s airflow, indoor air without aerosol spraying was used because aerosols could damage the O_3 monitor. Prior to the O_3 monitor experiments, it was verified that aerosol spraying did not produce a measurable change in the relative humidity of air flowing at 1 m/s inside the duct by comparing the relative humidity inside the duct before and during saline solution spraying for 30 minutes. This independence of humidity from aerosol spraying provided a theoretical basis for ensuring that O_3 monitor measurements obtained under clean airflow conditions represented the O_3 concentration during airborne bacteria collection experiments. The indoor air temperature and relative humidity during the O_3 monitor experiments were maintained within the ranges of 21–23 °C and 45–55%, respectively.

However, use of the O_3 monitor was unsuitable under zero duct airflow conditions because it required a flow rate of 1.5 L/min. Therefore, a UV–visible absorption spectroscopy system was established to measure the O_3 concentration within the ESP–SDBD filter *in situ.* Unfortunately, by the time the experimental setup had been modified for *in situ* spectroscopy, seasonal changes had resulted in drier air conditions. Consequently, the air temperature and relative humidity during the *in situ* O_3 measurement experiments were within the ranges of 21–23 °C and 32–38%, respectively. Therefore, the *in situ* O_3 measurement results were used to elucidate the inactivation mechanism within the ESP–SDBD filter but may differ from the O_3 concentrations present during the collected bacteria inactivation experiments.

Preparation of bacterial suspension and aerosol generation

Gram-negative *E. coli* (KCTC 1039) and Gram-positive *M. luteus* (KCTC 3063) were used as representative airborne bacteria. Both strains were streaked onto tryptic soy agar (TSA). *E. coli* plates were incubated at 37 °C for 24 hours, whereas *M. luteus* plates were incubated at 30 °C for 72 hours. A single colony from each plate was then inoculated into tryptic soy broth (TSB) and incubated overnight at the respective temperatures with shaking at 160 rpm. The resulting overnight cultures were mixed with sterile glycerol to a final concentration of 15% (w/w), aliquoted into sterile cryovials, and stored at −70 °C in a deep freezer as stock cultures.

For each experiment, a frozen stock culture was thawed and inoculated into TSB. The cultures were incubated for 20 hours at 37 °C for *E. coli* or 30 °C for *M. luteus* with shaking at 160 rpm. The cells were harvested and washed twice with sterile physiological saline (0.85% w/v) by centrifugation at 2,800 × g for 15 minutes at 4 °C (Labogene, 1580R). The cell density was adjusted with saline to a final concentration of 108–109 CFU/mL. This suspension was used as the feed solution for aerosol generation. A compressed-air atomiser (Topas GmbH, ATM 220) generated bacterial aerosols at 4.2 L/min using an inlet pressure of 4.8 bar. During each experiment, only one bacterial species was atomised, and the suspension was gently stirred at regular intervals to minimise sedimentation and maintain a uniform bacterial concentration.

Quantification of airborne bacteria

Airborne viable bacteria were sampled downstream of the ESP–SDBD section using a six-stage Andersen cascade impactor (Tisch Environmental Inc., TE-10-800) operated at a flow rate of 28.3 L/min. Because airborne bacterial concentrations were extremely high in the absence of ESP operation, the sampling duration for the control and SDBD operation was set to 8 seconds for *E. coli* and 6 seconds for *M. luteus* to prevent excessive colony loading. In contrast, when the ESP was activated (ESP and ESP + SDBD operation), the sampling time was extended to 120 seconds to achieve a sufficiently low detection limit for viable cell measurements. TSA plates were fitted onto all six stages of the impactor prior to sampling. After collection, the plates were incubated at 37 °C for 24 hours for *E. coli* or at 30 °C for 72 hours for *M. luteus*, and colonies were enumerated. The actual number of airborne bacteria was calculated using the positive-hole correction method with reference to the standard correction table [62]. The concentration of airborne bacteria (CFU/m^3) was calculated from the corrected colony count and the sampled air volume using the following equation:

$$C = \frac{N}{Q \times T} \times 1000$$

where N is the total number of colonies, Q is the sampling flow rate (28.3 L/min), T is the sampling time (minutes), and the multiplication factor converts litres to cubic metres.

The LOD was defined as the concentration equivalent to one colony count observed at the maximum sampling volume and was calculated as follows:

$$LOD = \frac{1}{Q \times t} \times 1000$$

where t is the longest sampling duration used in this study (i.e., 120 seconds).

The removal efficiency was calculated as follows:

$$\text{Removal efficiency (\%)} = (1 - \frac{C_{\text{treatment}}}{C_{\text{control}}}) \times 100$$

where C_{control} and $C_{\text{treatment}}$ represent the viable airborne concentrations at the duct outlet without and with treatment, respectively. When colony counts were below the detection limit, the LOD was applied for concentration estimation as described above.

Quantification of surface-attached bacteria

Residual viable bacteria were recovered from the internal surfaces of the ESP and quantified. Two surface

regions were examined: the ESP charging section (charging plate, 63 cm^2) and the collecting section (collecting plate, 157.5 cm^2). Preliminary tests confirmed that aerosol deposition was symmetric across the ESP–SDBD filter, with the greatest deposition in the central channel (Channel 3) and the least deposition in the outermost channels (Channels 1 and 5) (Supplementary Fig. 5a). Based on these results, the inner surfaces of Channel 3—namely, the lower surfaces of the top plates and the upper surfaces of the bottom plates—were sampled to quantify surface-attached bacteria (Supplementary Fig. 5b). Surface sampling was performed using a swab kit (ELMEX, Pro-media ST-25 PBS). Each defined area was thoroughly swabbed using two perpendicular wiping passes (one horizontal and one vertical) to maximise collection efficiency. After sampling, the swab was placed into a tube containing 10 mL of phosphate-buffered saline (PBS) and vortexed for 20 seconds to release the collected microorganisms. The recovered suspension was serially diluted in saline, and appropriate dilutions were spread onto TSA plates. The plates were incubated at 37 °C for 24 hours for *E. coli* or at 30 °C for 72 hours for *M. luteus*. After incubation, colonies were enumerated, and the surface concentration of attached bacteria was calculated as follows:

$$\text{Surface concentration (CFU/cm}^2) = \frac{N \times D \times V_s}{A \times V_d}$$

where N is the colony count recovered on agar, D is the dilution factor, V_s is the suspension volume used for swab recovery (10 mL), V_d is the plated volume for enumeration (e.g., 1 mL or 0.1 mL), and A is the sampled surface area (63 or 157.5 cm^2).

Simulation of electric wind during ESP + SDBD operation

Simulation of the corona discharge, SDBD, and the resulting convective airflow induced by electrohydrodynamic force (i.e., electric wind[63,64]) within a single channel of the ESP–SDBD filter during ESP + SDBD operation under zero duct airflow conditions was performed to investigate the disinfection mechanism. The model was developed using the electrostatics, charge transport, and laminar flow interfaces in COMSOL Multiphysics® (version 6.3). An illustration of the simulation domain and boundary conditions is provided in Supplementary Fig. 6. When the drift of charge carriers under the electric field dominates over charge transport by neutral flow, the current conservation, current density, and Poisson equations can be

written as follows:

$$\nabla \cdot \mathbf{J} = S \tag{1}$$

$$\mathbf{J} = z\mu\rho\mathbf{E} \tag{2}$$

$$\varepsilon_0 \nabla^2 V = -\rho \tag{3}$$

where $\mathbf{J}$ is the current density (A/m^2), S is the current source term (A/m^3), z is the charge number, μ is the ion mobility (m^2/(V·s)), ρ is the space charge density (C/m^3), $\mathbf{E}$ is the electric field (V/m), ε_0 is the vacuum permittivity, and V is the electric potential (V) [65,66]. Assuming constant mobility μ and $S = 0$, Equations (1)–(3) can be coupled into the following transport equation:

$$\rho^2 - \varepsilon_0 \nabla V \cdot \nabla \rho = 0 \tag{4}$$

The boundary conditions for solving this equation were specified as $V = V_0$ at the charging and collecting plates and as an electric field described by Peek's law [67,68] at the charging wire for the corona discharge:

$$E_0 = 3 \times 10^6 \delta \left(1 + \frac{0.03}{\sqrt{\delta r_i}}\right) \tag{5}$$

where E_0 is the breakdown electric field (V/m), δ is the gas number density normalised to the gas density at 760 Torr and 293.15 K, and r_i is the radius of the charging wire. The boundary conditions representing the SDBD were simplified by assigning a uniform space charge density of -5×10^{-4} C/m^3 to 0.2 mm-wide discharge regions distributed across the SDBD unit surface. This estimate corresponds to a charge number density of 3.12×10^9 cm^{-3}, which is within a reasonable range given that charge number densities in atmospheric-pressure dielectric barrier discharges can exceed 1×10^{10} cm^{-3} [41]. Nevertheless, this simplification limits the interpretation of the simulation results to a qualitative illustration of the electric wind flow. Given these boundary conditions, Equation (4) was solved to obtain the space charge density ρ and electric field $\mathbf{E}$ throughout the computational domain.

Meanwhile, the steady-state Navier–Stokes equations can be written as follows:

$$\rho_\mathrm{f}(\mathbf{u} \cdot \nabla)\mathbf{u} = \nabla \cdot \left[-p\mathbf{I} + \mu_\mathrm{f}\left(\nabla\mathbf{u} + (\nabla\mathbf{u})^\mathbf{T}\right)\right] + \mathbf{F} \tag{6}$$

$$\nabla \cdot \mathbf{u} = 0 \tag{7}$$

where ρ_f is the fluid mass density (kg/m^3), $\mathbf{u}$ is the fluid velocity (m/s), μ_f is the dynamic viscosity (kg/(m·s)), and $\mathbf{F}$ is the volume force [69]. The electrohydrodynamic volume force $\mathbf{F}_\mathrm{EHD}$ exerted on the neutral fluid through

momentum transfer from charged particles is given by:

$$\mathbf{F}_{\mathrm{EHD}} = e(n_i - n_e)\mathbf{E} - k_{\mathrm{B}}\nabla n_i T_i - k_{\mathrm{B}}\nabla n_e T_e \quad (8)$$

where e is the elementary charge, n_i and n_e are the ion and electron number densities (m^{-3}), respectively, k_{B} is the Boltzmann constant, and T_i and T_e are the ion and electron temperatures (K), respectively [70]. When diffusion of charged particles is negligible compared with their drift in electric fields, the electrohydrodynamic volume force can be simplified to:

$$\mathbf{F}_{\mathrm{EHD}} = \rho\mathbf{E} \quad (9)$$

The space charge density ρ and electric field $\mathbf{E}$ obtained previously were substituted into Equation (9) to calculate $\mathbf{F}_{\mathrm{EHD}}$ which was subsequently used in Equations. (6) and (7) to determine the electric wind velocity field, $\mathbf{u}$.

Data availability

The datasets generated during and/or analysed during the current study are available from the corresponding author on reasonable request.

References

1. Atkinson, J. *Natural Ventilation for Infection Control in Health-Care Settings*. (World Health Organization, 2009).
2. Tellier, R., Li, Y., Cowling, B. J. & Tang, J. W. Recognition of aerosol transmission of infectious agents: a commentary. *BMC Infect. Dis.* **19**, 101 (2019).
3. WHO COVID-19 dashboard. *World Health Organization* https://data.who.int/dashboards/covid19/deaths (2026).
4. Long, A. & Ascent, D. World economic outlook. *International Monetary Fund* **177**, (2020).
5. Madhav, N. *et al.* Pandemics: risks, impacts, and mitigation. *Disease control priorities: improving health and reducing poverty. 3rd edition* (2017).
6. Knight-Jones, T. J. D. & Rushton, J. The economic impacts of foot and mouth disease–What are they, how big are they and where do they occur? *Prev. Vet. Med.* **112**, 161–173 (2013).
7. Singh, S., Vishwakarma, P. & Gupta, T. Review of current and future indoor air purifying technologies. *ACS ES&T Engineering* **4**, 2607–2630 (2024).
8. Air Pollution Control Technology Fact Sheet: Paper/Nonwoven Filter - HEPA, ULPA (EPA-452/F-03-023). *United States Environmental Protection Agency (EPA)* (2009).
9. Hansel, N. N. *et al.* Randomized clinical trial of air cleaners to improve indoor air quality and chronic obstructive pulmonary disease health: results of the CLEAN AIR study. *Am. J. Respir. Crit. Care Med.* **205**, 421–430 (2022).
10. James, C. *et al.* HEPA filtration improves asthma control in children exposed to traffic-related airborne particles. *Indoor Air* **30**, 235–243 (2020).
11. Lee, T., Kim, J.-H., Lee, J. & Kwon, E. E. Thermochemical processing for the sustainable disposal of spent filter waste. *Chemosphere* **369**, 143863 (2024).

12. Mittal, H., Parks, S. R., Pottage, T., Walker, J. T. & Bennett, A. M. Survival of microorganisms on HEPA filters. *Applied Biosafety* **16**, 163–166 (2011).
13. Miaskiewicz-Peska, E. & Lebkowska, M. Comparison of aerosol and bioaerosol collection on air filters. *Aerobiologia (Bologna).* **28**, 185–193 (2012).
14. Ayush Kadam. *Global HEPA Filters Market 2025 – 2034*. https://www.custommarketinsights.com/report/hepa-filters-market/ (2026).
15. Assadi, I. *et al.* Review on inactivation of airborne viruses using non-thermal plasma technologies: from MS2 to coronavirus. *Environmental Science and Pollution Research* **29**, 4880–4892 (2022).
16. Zhang, L. *et al.* In-duct grating-like dielectric barrier discharge system for air disinfection. *J. Hazard. Mater.* **435**, 129075 (2022).
17. Vaze, N. D. *et al.* Inactivation of bacteria in flight by direct exposure to nonthermal plasma. *IEEE transactions on plasma science* **38**, 3234–3240 (2010).
18. Nayak, G. *et al.* Rapid inactivation of airborne porcine reproductive and respiratory syndrome virus using an atmospheric pressure air plasma. *Plasma Processes and Polymers* **17**, 1900269 (2020).
19. Xia, T. *et al.* Inactivation of airborne viruses using a packed bed non-thermal plasma reactor. *J. Phys. D Appl. Phys.* **52**, 255201 (2019).
20. Park, J. Y. *et al.* Development of high durability plasma filter for air circulating disinfection system. *Current Applied Physics* **41**, 100–110 (2022).
21. Baek, K. H. *et al.* Instant inactivation of aerosolized SARS-CoV-2 by dielectric filter discharge. *PLoS One* **17**, e0268049 (2022).
22. Li, J. *et al.* Plasma air filtration system for intercepting and inactivation of pathogenic microbial aerosols. *J. Environ. Chem. Eng.* **11**, 110728 (2023).
23. Liao, X. *et al.* Inactivation mechanisms of non-thermal plasma on microbes: A review. *Food Control* **75**, 83–91 (2017).
24. Dobrynin, D., Fridman, G., Friedman, G. & Fridman, A. Physical and biological mechanisms of direct plasma interaction with living tissue. *New J. Phys.* **11**, 115020 (2009).
25. Adesina, K., Lin, T.-C., Huang, Y.-W., Locmelis, M. & Han, D. A review of dielectric barrier discharge cold atmospheric plasma for surface sterilization and decontamination. *IEEE Trans. Radiat. Plasma Med. Sci.* **8**, 295–306 (2024).
26. Kettleson, E. M. *et al.* Airborne virus capture and inactivation by an electrostatic particle collector. *Environ. Sci. Technol.* **43**, 5940–5946 (2009).
27. Wang, L. *et al.* Aerodynamic size-dependent collection and inactivation of virus-laden aerosol particles in an electrostatic precipitator. *Environ. Sci. Technol.* **58**, 16941–16951 (2024).
28. Zukeran, A. *et al.* Investigation of inactivation process for microorganism collected in an electrostatic precipitator. *J. Electrostat.* **93**, 70–77 (2018).
29. Mizuno, A. Electrostatic precipitation. *IEEE Transactions on dielectrics and electrical insulation* **7**, 615–624 (2002).
30. Chen, L., Gonze, E., Ondarts, M., Outin, J. & Gonthier, Y. Electrostatic precipitator for fine and ultrafine particle removal from indoor air environments. *Sep. Purif. Technol.* **247**, 116964 (2020).
31. Kim, H., Han, B., Kim, Y., Oda, T. & Won, H. Submicrometer particle removal indoors by a novel electrostatic precipitator with high clean air delivery rate, low ozone emissions, and carbon fiber ionizer. *Indoor Air* **23**, 369–378 (2013).
32. Jeong, S. Bin, Shin, J. H., Kim, S. W., Seo, S. C. & Jung, J. H. Performance evaluation of an electrostatic precipitator with a copper plate using an aerosolized SARS-CoV-2 surrogate (bacteriophage phi 6). *Environ. Technol. Innov.* **30**, 103124 (2023).
33. Tseng, C.-C. & Li, C.-S. Ozone for inactivation of aerosolized bacteriophages. *Aerosol science and technology* **40**, 683–689 (2006).
34. Timmermann, E. *et al.* Indoor air purification by dielectric barrier discharge combined with ionic wind: Physical and microbiological investigations. *J. Phys. D Appl. Phys.* **51**, 164003 (2018).
35. Prehn, F. *et al.* Inactivation of airborne bacteria by plasma treatment and ionic wind for indoor air cleaning. *Plasma processes and polymers* **17**, 2000027 (2020).
36. Neretti, G. *et al.* Geometry optimization of linear and annular plasma synthetic jet actuators. *J. Phys. D Appl. Phys.* **50**, 015210 (2016).
37. Jung, H., Kim, D.-B., Gweon, B., Moon, S.-Y. & Choe, W. Enhanced inactivation of bacterial spores by atmospheric pressure plasma with catalyst TiO2. *Appl. Catal. B* **93**, 212–216 (2010).

38. Mastanaiah, N., Banerjee, P., Johnson, J. A. & Roy, S. Examining the role of ozone in surface plasma sterilization using dielectric barrier discharge (DBD) plasma. *Plasma Processes and Polymers* **10**, 1120–1133 (2013).
39. Shu, J. *et al.* Synergistic generation of N2O5 by needle-ring electrode and gliding Arc discharge air plasmas for enhanced bacterial inactivation. *AIP Adv.* **15**, (2025).
40. Uhm, H. S. Influence of chamber temperature on properties of the corona discharge system. *Phys. Plasmas* **6**, 623–626 (1999).
41. Kang, W. S., Kim, H.-S. & Hong, S. H. Gas temperature effect on discharge-mode characteristics of atmospheric-pressure dielectric barrier discharge in a helium–oxygen mixture. *IEEE Transactions on Plasma Science* **38**, 1982–1990 (2010).
42. Robinson, M. Movement of air in the electric wind of the corona discharge. *Transactions of the American Institute of Electrical Engineers, Part I: Communication and Electronics* **80**, 143–150 (1961).
43. Müller, S., Zahn, R. & Grundmann, J. Extraction of ions from dielectric barrier discharge configurations. *Plasma Processes and Polymers* **4**, S1004–S1008 (2007).
44. Müller, S. & Zahn, R. Air pollution control by non-thermal plasma. *Contributions to Plasma Physics* **47**, 520–529 (2007).
45. Jidenko, N., Mathon, R., Gérard, V., Adédiran, A. M. & Borra, J.-P. Dielectric barrier discharge as bipolar ion source for aerosol charging: Application to filtration, thin film, and aerosol size measurement. *J. Electrostat.* **126**, 103856 (2023).
46. Bruggeman, P. & Brandenburg, R. Atmospheric pressure discharge filaments and microplasmas: physics, chemistry and diagnostics. *J. Phys. D Appl. Phys.* **46**, 464001 (2013).
47. Bruins, A. P. Mass spectrometry with ion sources operating at atmospheric pressure. *Mass Spectrom. Rev.* **10**, 53–77 (1991).
48. Huertas, M. L., Marty, A. M., Fontan, J., Alet, I. & Duffa, G. Measurement of mobility and mass of atmospheric ions. *J. Aerosol Sci.* **2**, 145–150 (1971).
49. Filters. *OC IMP Klima* https://www.oc-impklima.com/application/files/2616/6790/2946/Filters_Nov2022_ENG.pdf (2022).
50. Organization, W. H. *WHO Global Air Quality Guidelines: Particulate Matter (PM2.5 and PM10), Ozone, Nitrogen Dioxide, Sulfur Dioxide and Carbon Monoxide*. (World Health Organization, 2021).
51. Ozone National Ambient Air Quality Standards (NAAQS). *United States Environmental Protection Agency* https://www.epa.gov/ground-level-ozone-pollution/ozone-national-ambient-air-quality-standards-naaqs (2020).
52. Radalj, A. *et al.* Combating pathogens using carbon-fiber ionizers (CFIs) for air purification: A narrative review. *Applied Sciences* **14**, 7311 (2024).
53. Kim, H.-J., Han, B., Woo, C. G. & Kim, Y.-J. Ozone emission and electrical characteristics of ionizers with different electrode materials, numbers, and diameters. *IEEE Trans. Ind. Appl.* **53**, 459–465 (2016).
54. Kikuchi, Y., Miyamae, M., Nagata, M. & Fukumoto, N. Effects of environmental humidity and temperature on sterilization efficiency of dielectric barrier discharge plasmas in atmospheric pressure air. *Jpn. J. Appl. Phys.* **50**, 01AH03 (2011).
55. Zhang, X., Lee, B. J., Im, H. G. & Cha, M. S. Ozone production with dielectric barrier discharge: effects of power source and humidity. *IEEE transactions on plasma science* **44**, 2288–2296 (2016).
56. Ki, S. H., Masur, K., Baik, K. Y. & Choi, E. H. Effects of humidity on room disinfection by dielectric barrier discharge plasma. *J. Phys. D Appl. Phys.* **52**, 425204 (2019).
57. Avino, F. *et al.* Surface DBD degradation in humid air, and a hybrid surface-volume DBD for robust plasma operation at high humidity. *J. Phys. D Appl. Phys.* **56**, 345201 (2023).
58. Huh, S.-C. *et al.* Individual quantification of ozone and reactive nitrogen species in mixtures by broadband UV–visible absorption spectra deconvolution. *Plasma Sources Sci. Technol.* **33**, 075007 (2024).
59. Zhang, X., Lee, B. J., Im, H. G. & Cha, M. S. Ozone production with dielectric barrier discharge: effects of power source and humidity. *IEEE transactions on plasma science* **44**, 2288–2296 (2016).
60. Ki, S. H., Masur, K., Baik, K. Y. & Choi, E. H. Effects of humidity on room disinfection by dielectric barrier discharge plasma. *J. Phys. D Appl. Phys.* **52**, 425204 (2019).
61. Kikuchi, Y., Miyamae, M., Nagata, M. & Fukumoto, N. Effects of environmental humidity and

temperature on sterilization efficiency of dielectric barrier discharge plasmas in atmospheric pressure air. *Jpn. J. Appl. Phys.* **50**, 01AH03 (2011).
62. Macher, J. M. Positive-hole correction of multiple-jet impactors for collecting viable microorganisms. *Am. Ind. Hyg. Assoc. J.* **50**, 561–568 (1989).
63. Park, S., Cvelbar, U., Choe, W. & Moon, S. Y. The creation of electric wind due to the electrohydrodynamic force. *Nat. Commun.* **9**, 371 (2018).
64. Park, S. *et al.* Stabilization of liquid instabilities with ionized gas jets. *Nature* **592**, 49–53 (2021).
65. Adamiak, K. & Atten, P. Simulation of corona discharge in point–plane configuration. *J. Electrostat.* **61**, 85–98 (2004).
66. *Plasma Module User's Guide (v6.4)*. (COMSOL, 2024).
67. Peek, F. W. *Dielectric Phenomena in High-Voltage Engineering*. (McGraw-Hill Book Company, Incorporated, 1929).
68. Kuffel, J. & Kuffel, P. *High Voltage Engineering Fundamentals*. (Elsevier, 2000).
69. Batchelor, G. K. *An Introduction to Fluid Dynamics*. (Cambridge university press, 2000).
70. Boeuf, J. P. & Pitchford, L. C. Electrohydrodynamic force and aerodynamic flow acceleration in surface dielectric barrier discharge. *J. Appl. Phys.* **97**, 103307 (2005).

Acknowledgements

This work was supported by the Korea Advanced Institute of Science and Technology (No. N10260034), the National Research Foundation of Korea (No. 00407018), and the Korea Institute of Materials Science (No. PNKA950 and PNKB020).

Author contributions

S.C.H.: Writing – original draft, Conceptualization, Formal analysis, Investigation, Methodology, Software, Visualization. K.H.B.: Writing – original draft, Formal analysis, Investigation, Methodology. T.K.: Investigation. J.C.: Investigation. J.Y.P.: Writing – review & editing, Project administration, Resources. W.C.: Writing – review & editing, Conceptualization, Formal analysis, Project administration, Funding acquisition, Supervision.

Competing interests

Seong-Cheol Huh and Wonho Choe have filed a patent application (10-2025-0004530) for the ESP–SDBD filter concept and are pursuing patent registration.

Figures

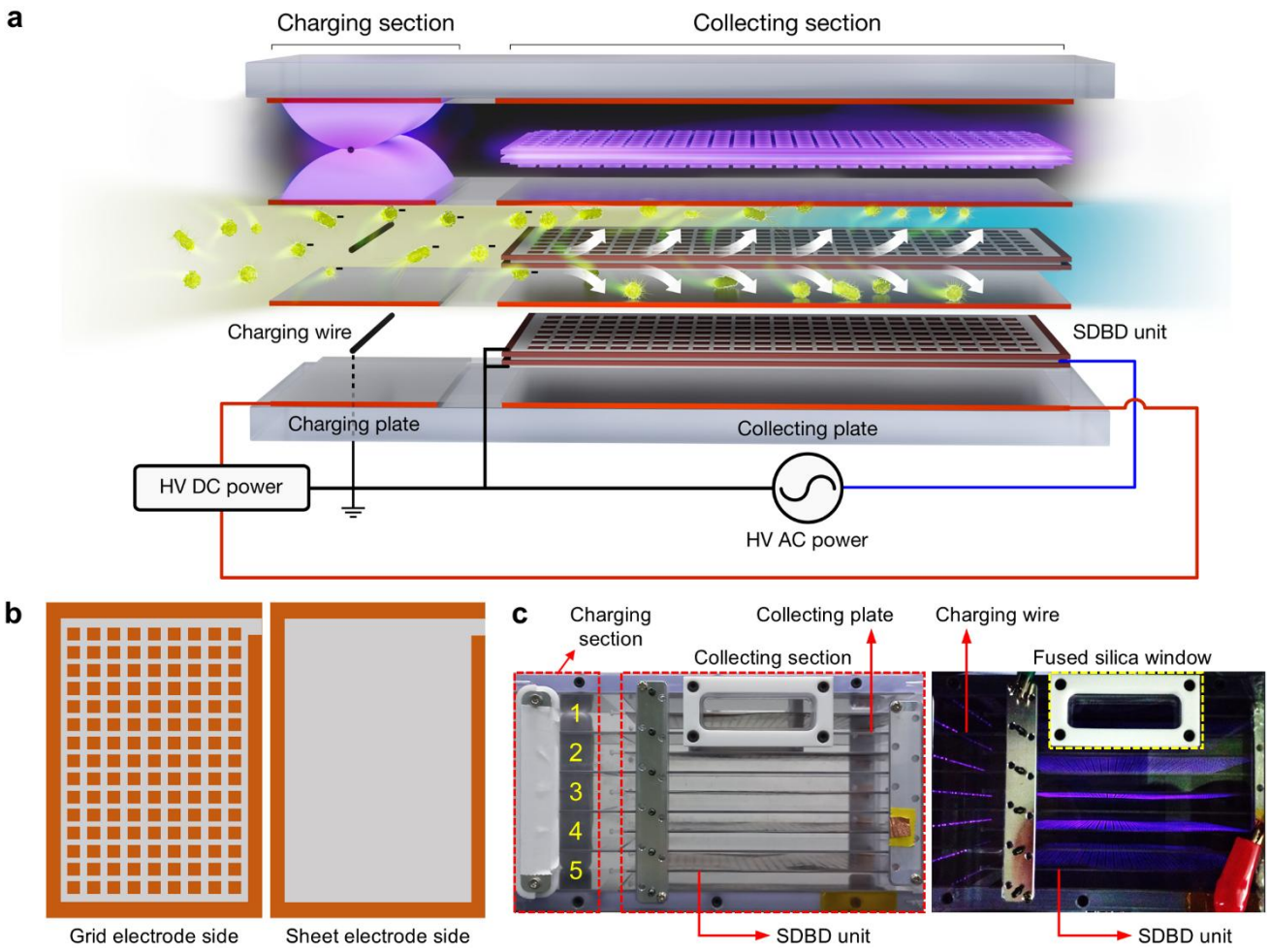

Fig. 1 | ESP–SDBD plasma filter concept and structure. a, Concept and operation of the ESP–SDBD filter. The three channels illustrated represent the plasma generation region, the pathogen collection mechanism, and the electrical circuitry, respectively. **b**, Schematic of the SDBD sources. **c**, The ESP–SDBD plasma filter without plasma discharge and during plasma operation. The numbers in the charging section indicate the numbering of the five identical channels.

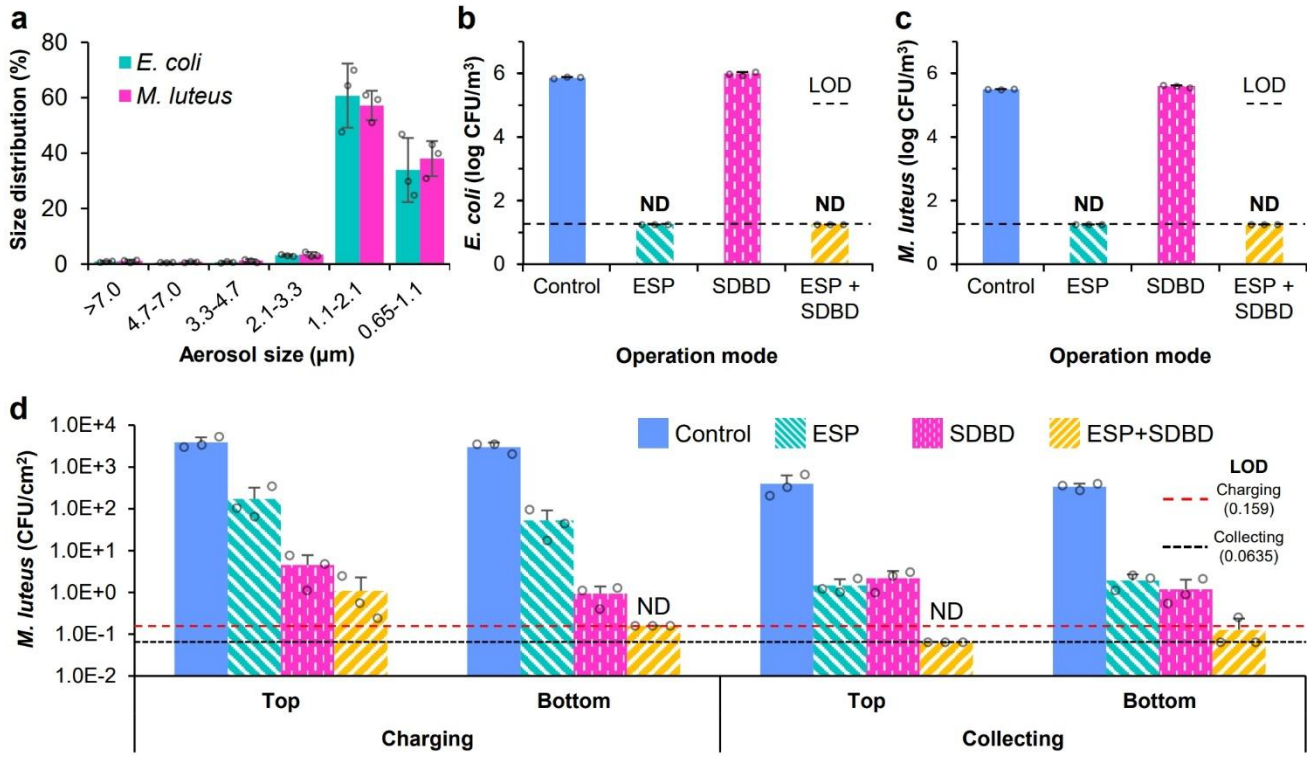

768

769 **Fig. 2 | Bacterial aerosol collection and inactivation results. a**, Aerosol size distributions of *E. coli* and *M.*
770 *luteus*. **b**, Downstream viable *E. coli* concentration in the outflowing airstream during airborne bacteria
771 collection experiments. **c**, Downstream viable *M. luteus* concentration in the outflowing airstream during
772 airborne bacteria collection experiments. Airborne bacteria were not detected (ND) downstream of the ESP–
773 SDBD filter under ESP and ESP + SDBD operating conditions. **d**, Surface-associated *M. luteus* remaining
774 after the collected bacteria inactivation experiment. The error bars represent the standard deviation of triplicate
775 experiments.

776

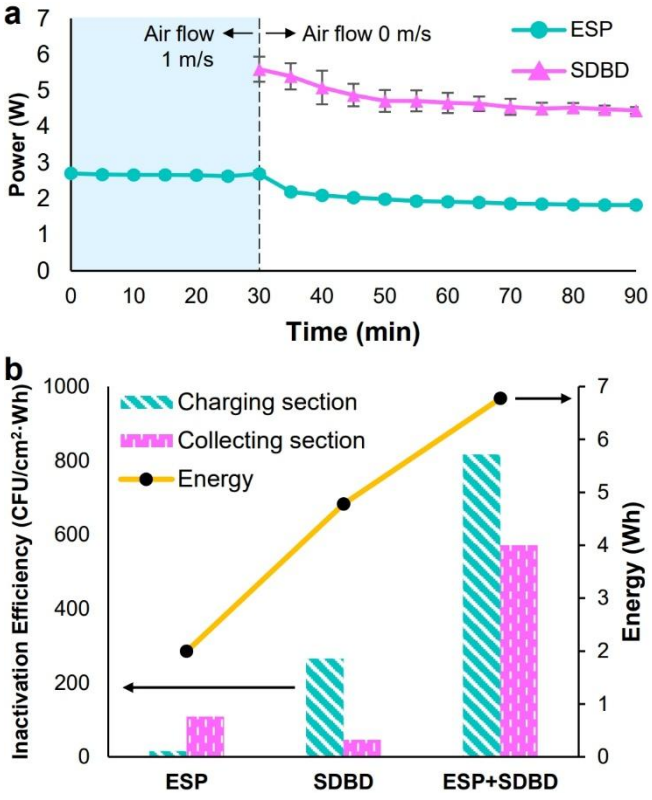

Fig. 3 | ESP–SDBD filter power consumption and energy efficiency. a, Power consumption of the ESP and SDBD components of the ESP–SDBD filter during the collected bacteria inactivation experiments. The error bars represent the standard deviation of triplicate experiments. **b**, Inactivation efficiency of collected *M. luteus* and energy consumption for inactivation under each ESP–SDBD filter operating mode.

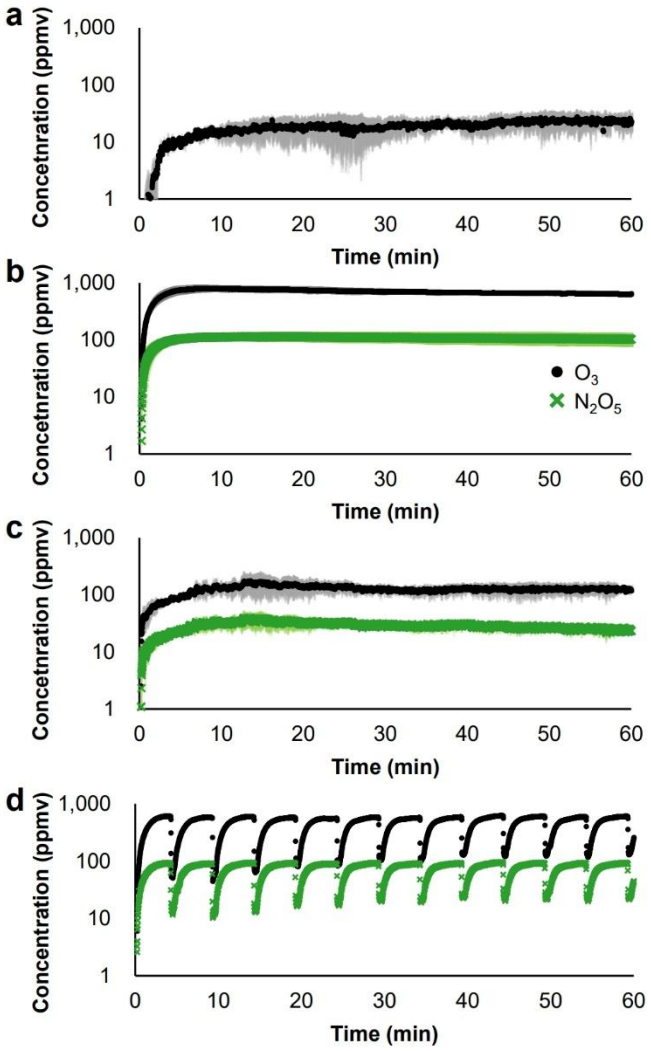

Fig. 4 | Measured *in situ* O_3 and N_2O_5 concentrations. Results for **a**, ESP; **b**, SDBD; and **c**, ESP + SDBD operating modes during the collected bacteria inactivation experiments. The lightly shaded error bars represent the standard deviation of triplicate experiments. **d**, Measured *in situ* O_3 and N_2O_5 concentrations during the ESP switching experiment. The switching experiment was conducted once.

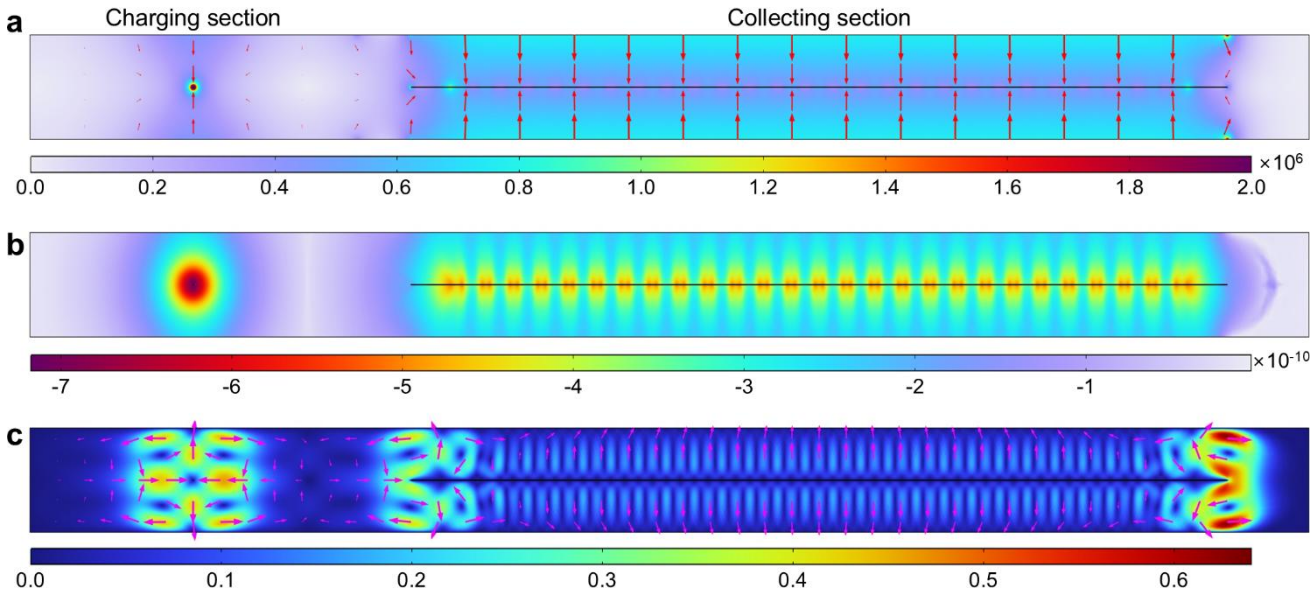

Fig. 5 | Simulation results of electric wind during ESP + SDBD operation. a, Electric field, **E** (V/m). **b**, Space charge density, ρ (C/cm^3). **c**, Electric wind velocity field, **u** (m/s). This simulation model provides a qualitative illustration of the electric wind physics within the ESP–SDBD filter. Directional electric wind flow from the corona discharge towards the charging plates in the charging section, and from the SDBD plasma towards the collecting plates in the collecting section are visible in **c**.

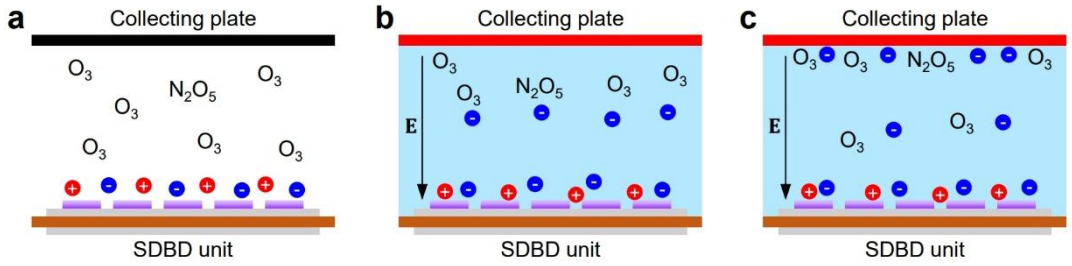

Fig. 6 | Mechanism of electric wind from the SDBD unit to the collecting plate surfaces. a, SDBD operation. Reactive species such as O_3 or N_2O_5 produced by the SDBD diffuse into the gap, while ions remain concentrated near the SDBD surface. **b**, Transition from SDBD operation to ESP + SDBD operation. As an electric field (**E**) is established, negative ions begin to drift towards the collecting plate, transferring momentum to neutral particles and generating an electric wind from the SDBD unit to the collecting plate. This electric wind transports reactive species towards the collecting plate, thereby rapidly decreasing the reactive species concentration within the gap. **c**, Continued ESP + SDBD operation. The SDBD plasma continuously generates reactive species and ions, which are transported to the collecting plate surfaces. This enhanced transport of reactive species towards the collecting plates during ESP + SDBD operation explains the lower reactive species concentrations and the more efficient bacterial inactivation observed under ESP + SDBD operation.

Tables

Table 1. Reduction efficiency (CFU/(cm^2·Wh)) of *M. luteus* by the ESP–SDBD filter

All energy consumption and reduction values used in the calculations were averaged from three independent experiments. For the energy values, 1.995, 4.78, and 6.78 Wh were used for the ESP, SDBD, and ESP + SDBD operating modes, respectively. For not detected (ND) cases under the ESP + SDBD condition, the LOD was substituted for the reduction calculation. The data presented in this table correspond to those shown in Fig. 3b.

Operation mode	Charging section	Collecting section
ESP	15.44	108.5
SDBD	266	46.0
ESP + SDBD	817	572

Supplementary Files

This is a list of supplementary files associated with this preprint. Click to download.

- Nat.Commun.SupplementaryMaterial.pdf